

## **Rheology and Flow Behavior of Concentrated Colloidal Gels for Direct-Write Assembly of 3D Mesoscale Structures**

Cheng Zhu and James E. Smay

School of Chemical Engineering, Oklahoma State University, Stillwater, OK, 74078

### **Abstract**

3D mesoscale structures with various patterns have been successfully fabricated by direct-write assembly of concentrated colloidal gels. Geometric fidelity of these structures is very important to functionality as devices and has been closely tied to gels microstructure dynamics, which depends on the rheology and shear history. Here,  $\text{Al}_2\text{O}_3$  gels were prepared and employed as model materials. A thixotropic rheological model was developed to show the time dependent behavior of gels structure during shear flow. The model accounts for structure formation and attrition, each with a shear history dependent rate constant. The true wall stress was measured by correcting the end effects and wall slip. The extrusion flow dynamics of the gel was simulated by using CFD method to disclose the structure profiles of extrusion filaments and predict the structure evolution of as-deposited filaments.

### **Introduction**

Extrusion-based direct-write process [1, 2] have successfully assembled the intricate 3D mesoscale (100 ~ 1000  $\mu\text{m}$ ) structures, which have widely potential applications in sensors [3, 4], photonic band-gap materials [5], microvascular networks [6], and tissue-engineering scaffolds [7, 8]. This process continuously extrudes gel-based ink filament from a deposition nozzle system to draw complex patterns by the sequential delivery of ink materials in a layer-by-layer manner without traditional part-specific tooling, dies or molds [3-5]. The shear thinning behavior of colloidal inks facilitates extrusion flow through fine capillary tubes, and their rapid transition from a flowable fluid to a strong elastic solid upon removal of extrusion pressure contributes to maintain desired structures shape after deposition [2, 9]. Although colloidal inks possess excellent self-supporting properties, the deposited structures are still inevitably subject to shape deformation due to gravity and colloidal microstructures evolution during deposition and afterwards and this has been closely tied to ink rheological properties, as well as shear history [9]. Thorough understanding of colloidal inks rheology provides useful information to convey an accurate description of inks structure evolution during deposition and thereafter. It is very helpful to improve the geometric fidelity of micro devices to ensure their physical functionality.

Previous studies have attributed the equilibrium shape deformation to the equilibrium elastic modulus of ink materials [2]. Despite the accuracy of this method in describing the equilibrium shape of deposited structures, it is still uncertain how the complex rheology of colloidal inks will affect dynamic shape evolution of as-deposited structures. Morissette and Lewis [10, 11] first calculated the shear rate profile in the extrusion filament by assuming the ink material as Newtonian fluids. Smay et al., [2] used Herschel-Bulkley model to simulated the capillary flow dynamics of PZT colloidal inks and raised a core-shell architecture as a result of a radically varying shear stress within the extrusion nozzle. These investigations treated inks as time-independent materials, and the simulation results indicated that extrudate was in a state of non-equilibrium only during extrusion and recovers at once upon deposition. Besides, no-slip wall boundary conditions were always adopted in these studies for Newtonian or simple rheological fluids flow dynamics [2, 10-13]. However, recent studies such as, direct flow visualization, finite element modeling, and classical fluid mechanics indicated that the colloidal structure is actually in a state of transition during extrusion and afterwards [12, 13]. Moreover, previous

experience showed that both the extrusion flow in the capillary tube and the shape evolution after deposition occurs only in several few seconds [2]. It can be deduced that the short duration unsteady state flow behavior is of significance in this case.

Since concentrated colloidal inks generally display strong viscoelastic behavior, it is difficult sometimes to distinguish the effect of thixotropy from that of viscoelasticity clearly [14]. The thixotropic rheology of colloidal inks over shorter time scales seems to be critically important from the perspective of colloidal structures evolution during flow dynamics and after deposition. Recently, structural kinetic models have been successfully applied to describe the thixotropic rheology of numerous colloidal dispersions or weakly flocculated suspensions with low solid volume fraction [15-21]. And this is the first time to analyze the thixotropy of concentrated colloidal gels with viscoelastic properties using this method. Besides, the rheologically complex fluids are known to violate the no-slip boundary conditions [22]. During the extrusion process, wall slip of the gel is thought to occur due to a thin solvent rich, but particle depleted layer near the deposition nozzle wall [23]. In this paper, concentrated  $\text{Al}_2\text{O}_3$  colloidal gels were employed as a model ink material to investigate the thixotropic rheology as the first step of a series of shape evolution experiments. A relatively simple and practical engineering model based on the structural kinetics theory was proposed to quantify viscoelastic thixotropy of  $\text{Al}_2\text{O}_3$  colloidal gels. Then, this model was used to simulate the inks flow dynamics and structure evolution. A series of extrusion pressure experiments were carried out to determine the wall slip effect to accurately convey the flow dynamics information. In subsequent research, the structure evolution of as-deposited gels will be correlated to the dynamic shape evolution of 3D structures.

## Experimental

### *Materials and gels preparation*

Aluminum oxide powders (AKP-30, Sumitomo Chemical Co., Tokyo, Japan, with a mean particle size of  $0.32\ \mu\text{m}$ , a specific surface area of  $7.1\ \text{m}^2/\text{g}$ , and a density of  $3.97\ \text{g}/\text{cm}^3$ ) served as ceramic phase. A 40% aqueous solution of poly(acrylic acid) (PAA) (Darvan 821A, R.T. Vanderbilt Co., Norwalk, CT) was used as a dispersant. Hydroxypropyl methylcellulose (HPMC) (Methocel F4M, Dow Chemical Co., Midland, MI, with a molecular weight of 3500) was prepared in a 5wt% stock solution and used as a viscosifier. Nonlinear poly(ethylenimine) (ICN Biomedical, Aurora, OH, with molecular weight of 50,000~100,000) ( $\text{PEI}_{50-100\text{k}}$ ) were prepared in aqueous stock solutions with 10% polymer weight, and served as flocculants. All samples were prepared in de-ionized water having a nominal conductivity of  $5 \times 10^{-4}\ \Omega^{-1}\ \text{cm}^{-1}$ .

Concentrated  $\text{Al}_2\text{O}_3$  colloidal gels preparation follows a two-step procedure. First, Darvan 821A (0.65 wt%, based on alumina weight), de-ionized water, and alumina powders were added sequentially into a 250ml sample cup containing about 30g of 3mm diameter zirconia milling media. The blend was mixed for 3min in a non-contact mixer (AR-250, Thinky Co., Laguna Hills, CA) to obtain a high concentrated colloidal suspension. Next, HPMC was added to achieve 7mg/ml in the liquid phase. After mixed for 1.5min and kept equilibrium for 1hr, these suspensions were gelled by adding the flocculant of 10wt%  $\text{PEI}_{50-100\text{k}}$  solution, to achieve a desired flocculant concentration.

### *Rheological measurements*

Two rheological measurements (i.e., shear rate step-change experiment, and hysteresis loop experiment) were adopted to test the thixotropic behavior of model materials [14, 17, 24]. The first set of experiments consisted of a series of continuous shear rate step changes. The shear

rate  $\dot{\gamma}$  was suddenly increased or decreased from a previous steady state to a new value until reaching a new steady state. All measurements were maintained for 1 min, which was sufficient to attain the steady state in all cases. The second set of experiments consisted of hysteresis loops with different sweep times, where the shear rate was linearly increased from none to  $100\text{s}^{-1}$  and decreased to zero at the same speed. All measurements were performed with a rheometer (Model Bohlin C-VOR 200, Bohlin Instruments, East Brunswick, NJ) under the isothermal condition at  $25^{\circ}\text{C}$  by digital temperature controller.

#### *Extrusion pressure measurements*

The analysis of wall slip requires a precise determination of the true wall stress  $\tau_w$ . Since the syringe barrel has a significantly larger diameter than that of the nozzle, it is important to correct the pressure loss at the entrance of the nozzle to specify the wall stress. Bagley correction [25] was performed here by using data from nozzles of same diameter but different length. The  $\tau_w$  after Bagley correction can be expressed as:

$$\tau_w = \frac{D\Delta P}{4(L+e)} \quad (1)$$

where  $e$  is the equivalent length caused by ends effect. And it can be determined by extrapolating  $\Delta P$  versus the  $L$  curve to  $L = 0$ . Since the flow rate is another influence factor to the excess pressure drop due to these end effects [26], various average extrusion velocities  $V_{ave}$  were performed. Here, we use apparent shear rate  $\dot{\gamma}_a$  as controllable variable, and it can be related to the  $V_{ave}$  as  $\dot{\gamma}_a = \frac{8V_{ave}}{D}$ .

Table 1. Dimensions of extrusion system and operation conditions

Syringe diameter, $D_0$ (mm)	9.6
Nozzle diameter, $D$ (mm)	0.2
Nozzle length, $L$ (mm)	6.3, 12.7, 19.1
Average extrusion velocity, $V_{ave}$ (mm/s)	1, 2, 4, 8, 12

The extrusion pressures were measured by using a robotic deposition apparatus (Robocaster, Oklahoma State University, Stillwater, OK), a pressure transducer (load cell, LCGD 25, OMEGA Engineering Inc., Stamford, CT), and data conversion and acquisition systems. The sample material was loaded into a 3cc syringe barrel (Nordson EFD, East Providence, RI) fitted with extrusion nozzles (Nordson EFD, East Providence, RI) with varying length. The plunger of robocaster was connected to the load cell, and pushed the ram downward to extrude the gel at a fixed velocity. The load cell between the plunger and the ram measured the applied force and transfer the data to the data acquisition system. The dimensions of the components and operation conditions were listed in Table 1.

### **Theoretical Model of and Numerical Simulation**

#### *Structural kinetics*

We follow the classic structural kinetic theory to propose a normalized structural parameter,  $\lambda(\dot{\gamma}, t)$  (i.e.,  $0 \leq \lambda \leq 1$ ), to describe the thixotropic behavior of the gel. A fully structured gel has  $\lambda = 1$ , whereas a stable colloidal sol has  $\lambda = 0$ . The evolution of  $\lambda$  is assumed to be a first-order rate equation controlled by the flocs structure breakdown rate and agglomeration rate during the shear flow. The breakdown rate is assumed to be proportional to the instantaneous breakdown probability (i.e.,  $\lambda$ ), while the agglomeration rate is assumed to be proportional to the instantaneous agglomeration probability (i.e.,  $1 - \lambda$ ). Thus, the structural kinetic equation can be written as [20, 27, 28]:

$$\frac{\partial \lambda(\dot{\gamma}, t)}{\partial t} = -K_b \lambda + K_a (1 - \lambda) \quad (2)$$

where  $K_b$  is the overall breakdown rate constant,  $K_a$  is the overall agglomeration rate constant. The breakdown rate is the product of collision frequency and probability of breakdown. Since collision frequency is proportional to  $\dot{\gamma}$  [28, 29],  $K_b$  is assumed to be proportional to  $\dot{\gamma}$  as [28]:

$$K_b = k_b \dot{\gamma} \quad (3)$$

where  $k_b$  is specific breakdown rate constant. The agglomeration rate should increase with the  $\dot{\gamma}$  increase due to collision frequency and agglomeration probability increase. However, Gautham and Kapur [30] raised that higher shear rates will reduce the duration of collision significantly to make the agglomeration rate decrease eventually to zero. This  $K_a$  can be expressed as [30]:

$$K_a = \frac{k'_a \dot{\gamma} + k_0}{k''_a \dot{\gamma}^\rho + 1} \quad (4)$$

where  $k'_a$  and  $k''_a$  are specific agglomeration rate constant,  $\rho$  is a exponential factor ( $\rho > 1$ ), and  $k_0$  is a Brownian motion induced agglomeration rate constant.

Once the colloidal system achieves equilibrium at a given  $\dot{\gamma}$ , the agglomeration rate will equal the breakdown rate, and the structure of the system will approach an equilibrium value (i.e.,  $\lambda_e$ ). This dynamic balance can be expressed as:

$$K_a (1 - \lambda_e) = K_b \lambda_e \rightarrow \lambda_e = \frac{K_a}{K_a + K_b} \quad (5)$$

By integrating Eq. (2) and substituting Eq. (5), the  $\lambda$  has the following form as:

$$\lambda = \lambda_e + (\lambda_i - \lambda_e) \exp[-(K_a + K_b) t] \quad (6)$$

where  $\lambda_i$  is the structural parameter value prior to the  $\dot{\gamma}$  changes, (i.e.,  $\lambda(t = 0) = \lambda_i$ ).

#### *Constitutive relationship*

The elastic stress  $\tau^{el}$  and the viscous stress  $\tau^{vis}$  are decoupled as in Dullaert and Mewis model [20], and the total stress  $\tau_{total}$  of flocs structure is the sum of these two terms as:

$$\tau_{total} = \tau^{el} + \tau^{vis} \quad (7)$$

The  $\tau^{el}$  arising from the hydrodynamic interaction of the flocs, is assumed to obey a Hookean elastic response as:

$$\tau^{el} = G(\lambda) \gamma \quad (8)$$

where  $G(\lambda)$  is a structural dependent shear modulus, and  $\gamma$  is the elastic strain. The  $G(\lambda)$  is assumed to vary proportionally to the  $\lambda$  as [16, 20]:

$$G(\lambda) = \lambda G_0 \quad (9)$$

where  $G_0$  is the maximum shear modulus before shear flow starts (i.e.,  $\lambda = 1$ ). The  $\gamma$  will increase linearly from zero to some critical strain  $\gamma_c$  when the shear flow starts, and remain constant as long as the deformation process continues in the same direction [15]. It can be expressed as:

$$\gamma = \gamma_c \left[ 1 - \exp(-m \dot{\gamma} t^\alpha) \right] \quad (10)$$

where  $m$  and  $\alpha$  are characteristic parameters. For the simplicity, we define a maximum of elastic yield stress  $\tau_y$  as:

$$\tau_y = G_0 \gamma_c \quad (11)$$

The  $\tau^{el}$  can now be written as:

$$\tau^{\text{el}} = \lambda \tau_y \left[ 1 - \exp(-m\dot{\gamma}^\alpha) \right] \quad (12)$$

The  $\tau^{\text{vis}}$  originating from the transient flocs network, consists of two terms: one describes the apparent viscosity decay  $\eta_{\text{de}}(\lambda, \dot{\gamma})$  due to flocs structure breakdown, and the other describes the infinite apparent viscosity  $\eta_\infty$  at completely destroyed flocs structure ( $\lambda = 0$ ). It can be given as:

$$\tau^{\text{vis}} = \eta_{\text{de}}(\lambda, \dot{\gamma})\dot{\gamma} + \eta_\infty\dot{\gamma} \quad (13)$$

The viscosity decrement term  $\eta_{\text{de}}(\lambda, \dot{\gamma})$  is assumed to be proportional to  $\lambda$  and obey an exponential decay with the  $\dot{\gamma}$  as [31]:

$$\eta_{\text{de}}(\lambda, \dot{\gamma}) = \lambda \eta_0 \exp(-n\dot{\gamma}^\beta) \quad (14)$$

where  $\eta_0$  is zero-shear viscosity,  $n$  and  $\beta$  are material characteristic parameters. Hence, the constitutive equation can be written as:

$$\tau(\lambda, \dot{\gamma}) = \lambda \tau_y \left[ 1 - \exp(-m\dot{\gamma}^\alpha) \right] + \lambda \eta_0 \dot{\gamma} \exp(-n\dot{\gamma}^\beta) + \eta_\infty \dot{\gamma} \quad (15)$$

The instantaneous apparent viscosity  $\eta$  is defined as:

$$\eta = \frac{\tau_{\text{total}} - \tau^{\text{el}}}{\dot{\gamma}} = \lambda \eta_0 \exp(-n\dot{\gamma}^\beta) + \eta_\infty \quad (16)$$

Eq. (16) can also be applied to the equilibrium states, so we can get equilibrium apparent viscosity  $\eta_e$  as:

$$\eta_e = \lambda_e \eta_0 \exp(-n\dot{\gamma}^\beta) + \eta_\infty \quad (17)$$

### CFD simulation

By neglecting the inertia term, the mass and momentum conservation equations based on Navier-Stokes equations were used for simulation. The inlet boundary condition is fixed velocity and outlet boundary condition is fixed pressure. Two wall boundary conditions were considered: no-slip boundary and slip boundary conditions with constant wall stress obtained by extrusion pressure measurements. The commercial program COMSOL Multiphysics 3.5a (COMSOL, Burlington, MA) was used to solve the governing equations. The resolution is based upon an iterative Newton scheme. Convergence is achieved when norm of the change in solution vector between successive iterations is less than  $10^{-5}$ .

## Results and Discussion

### Steady state rheology

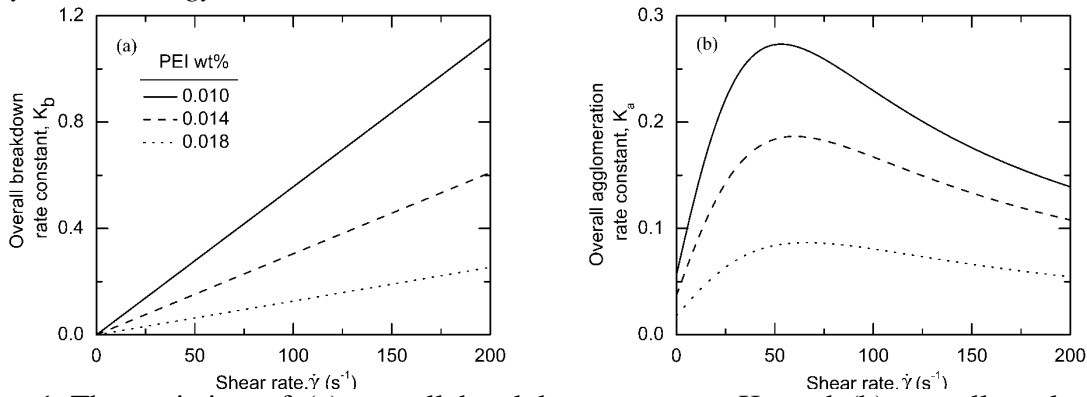


Figure 1 The variation of (a) overall breakdown constant  $K_b$  and (b) overall agglomeration constant  $K_a$  as a function of the shear rate  $\dot{\gamma}$ .

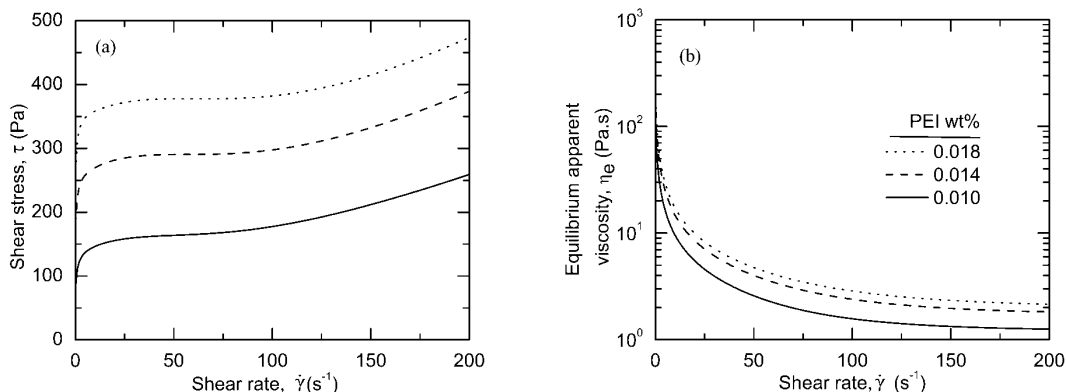


Figure 2 The steady state flow curves: (a) steady stress-shear rate curves, (b) steady apparent viscosity-shear rate curves.

Figure 1 showed the overall rate constant  $K_b$ , and  $K_a$  varies as a function of the  $\dot{\gamma}$ . We can see that  $K_b$  increases simply linearly along the  $\dot{\gamma}$ , while  $K_a$  shows initially increase until peak value and drop after that. The peak of the  $K_a$  is the transition point, where agglomeration rate changes from increment to decrement with the  $\dot{\gamma}$ . After obtaining the function of  $K_a$  and  $K_b$ , the  $\lambda_e$  can be calculated from Eq. (5), and the steady state flow curve can be predicted by substituting  $\lambda_e$  into Eq. (15). Figure 2 (a) shows the equilibrium flow curve of stress-shear rate relationship, and corresponding apparent viscosity-shear rate relationship also shows in Figure 2 (b). At higher  $\dot{\gamma}$ , the flow curve shows approximate Newtonian fluid characterization. The stronger gel shows higher yield stress, which implies a stronger elastic response.

#### Hysteresis loops

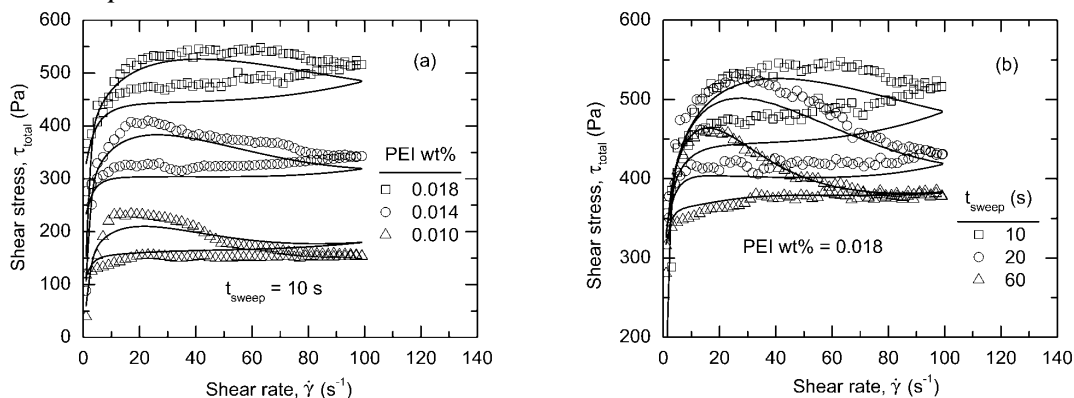


Figure 3 The hysteresis loops of experimental results comparing with model prediction: (a) varying PEI concentration at sweep time of 10 s, (b) at varying sweep times.

Hysteresis loops, observed in Figure 3 confirmed the thixotropic behavior of colloidal inks. The shear stress of the forward and backward curves encloses an area of hysteresis loops which indicates the thixotropy degree. In Figure 3 (a), the observed variation in hysteresis loops qualitatively revealed thixotropy increases with gel strength under the same sweep time. Figure 3 (b) showed the sweep times influence to the hysteresis loops. As the sweep time increased, the loops area decreased, and especially the down-curve approached the steady state flow curves. Although the hysteresis loops are not accurate enough for modeling, they have verified the shorter time-dependent behavior of colloidal gels.

### Breakdown and build-up curves

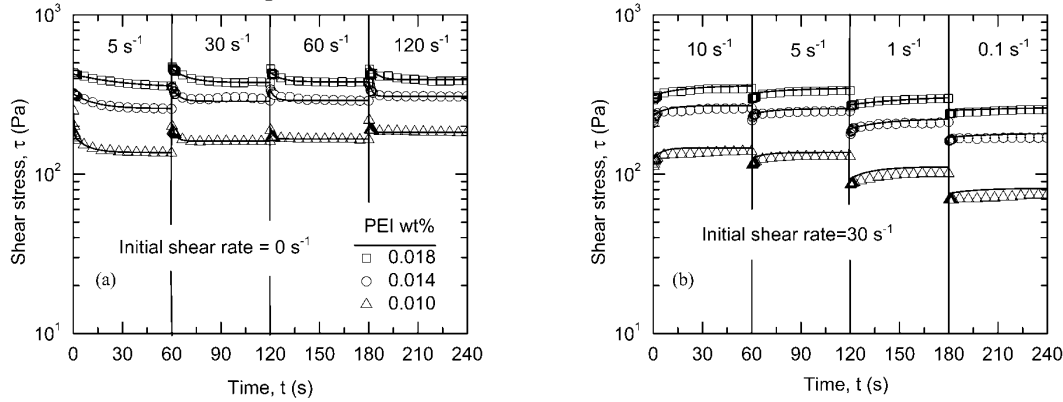


Figure 4 The shear rate step change of experimental results comparing with model prediction. (a) shear rate step-up measurements, (b) shear rate step-down measurements.

Figure 4 illustrated the continuous shear rate step change experimental results, compared with model predictions for  $\text{Al}_2\text{O}_3$  inks with varying PEI concentrations. In Figure 4 (a), the shear rate was suddenly applied to static sample inks and continuous increased to  $5$ ,  $30$ ,  $60$ , and  $120\text{s}^{-1}$ . At each step, the shear rate was retained for 1min to ensure to attain equilibrium. The initial shear stress overshoot was obvious, and relaxation time decreased as shear rate increased. Figure 4 (b) illustrated the shear stress as a function of shear rate step-down from initial  $30\text{s}^{-1}$  to  $10$ ,  $5$ ,  $1$ , and  $0.1\text{s}^{-1}$ . The shear stress recovered very fast from initial undershoots.

### Structural evolution after cessation of shear flow

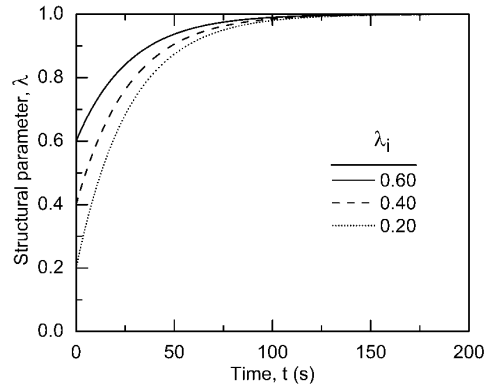


Figure 5 Structural parameter evolution for  $\text{Al}_2\text{O}_3$  inks of PEIwt% = 0.018 after cessation flow

After shear rates removed, the disrupted flocs can still aggregate at a specific rate with time toward the initially undisturbed value of structural parameter  $\lambda_e = 1$ . From Eq. (5) evolution of the structure parameter with no shear can be expressed by:

$$\lambda = 1 + (\lambda_i - 1) \exp(-k_0 t) \quad (18)$$

In Figure 5, the evolution of  $\lambda$  with time after cessation of shear flow was computed from Eq. (18) for different initial values of  $\lambda_i$ . The  $\lambda$  increased rapidly at beginning, and gradually slowed down until reached the maximum value eventually. It is obvious that the structural recovery path depends on  $\lambda_i$ , which can be altered by the prior history of the ink.

*Bagley end correction*

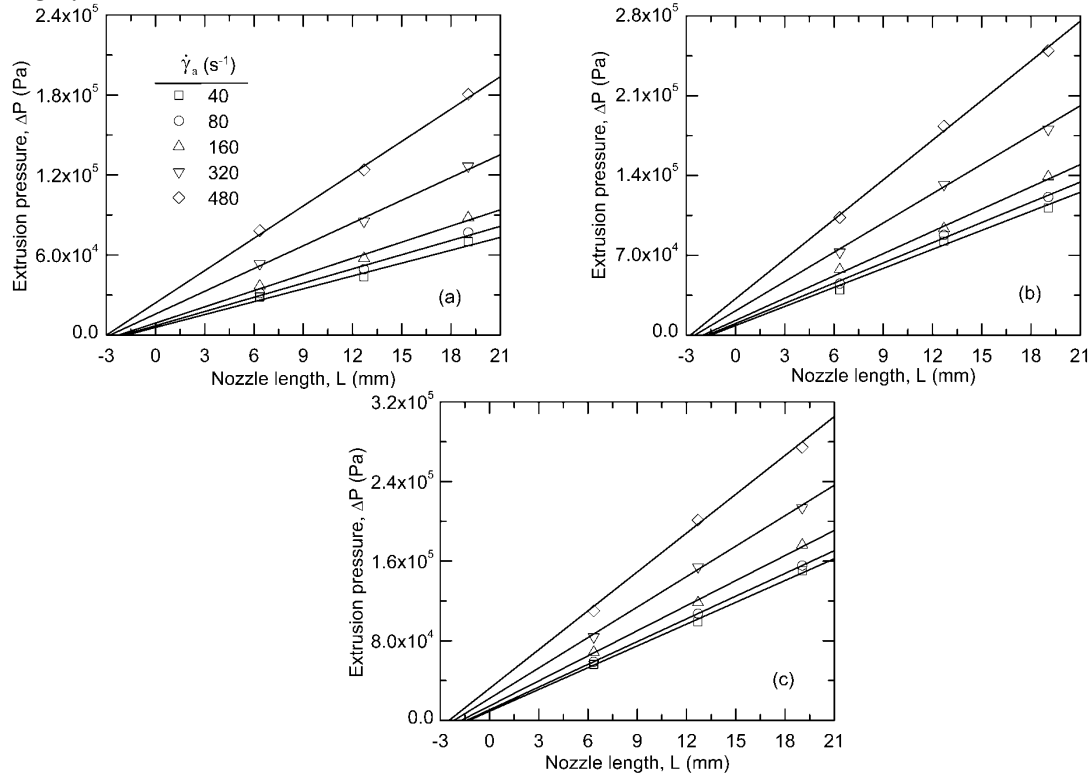


Figure 6 Bagley plots for  $\text{Al}_2\text{O}_3$  inks with varying PEIwt% = (a) 0.010, (b) 0.014, (c) 0.018.

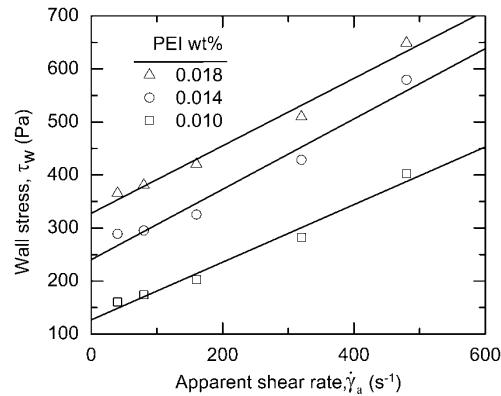


Figure 7 Computed  $\tau_w$  for  $\text{Al}_2\text{O}_3$  inks as a function of  $\dot{\gamma}_a$  extruded from nozzle of  $L = 12.7$  mm.

In Figure 6, the extrusion pressure drop  $\Delta P$  of three gels was plotted as a function of nozzle length  $L$  under various apparent shear rate  $\dot{\gamma}_a$ . The  $\Delta P$  values show excellent linear dependence on the  $L$  due to the small scatter of the results (less than 2%). All three gels show negative intercepts on the nozzle length axis, and this intercept is equivalent length  $e$  in Eq. (1). As the  $\dot{\gamma}_a$  increased, the equivalent length  $e$  increased correspondingly. That means higher inlet flow rate can intensify the end effects at the contraction entrance. Bagley correction can be successfully implemented according to Eq. (1) to compute the true wall stress  $\tau_w$  at varying  $\dot{\gamma}_a$ . Figure 7 shows the computed  $\tau_w$  approximately linear dependence on the  $\dot{\gamma}_a$  for three gels extruded from nozzles with length  $L = 12.7$  mm.

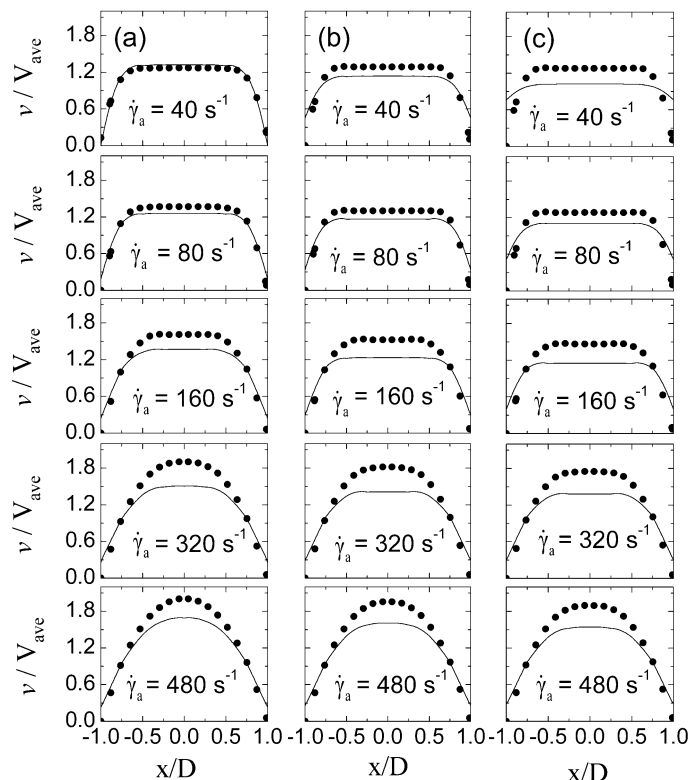


Figure 8 Dimensionless velocity profiles under various apparent shear rate compared with no-slip boundary condition CFD simulation results for three gels of varying PEIwt% = (a) 0.010, (b) 0.014, and (c) 0.018 extrusion flow in nozzles of 12.7 mm.

After obtaining the  $\tau_w$  as a function of  $\dot{\gamma}_a$ , the wall slip effects and bulk flow dynamics can be obtained and compared with the CFD simulation results with no slip wall conditions. Figure 8 shows the extrusion velocity  $v$  profiles as a function of the distance from the center  $x$  at the exit of the nozzle for varying  $\dot{\gamma}_a$ . Each flow profile is normalized by its average extrusion velocity  $V_{ave}$ , and plotted against the dimensionless position in the nozzle  $x/D$ . The dot line represents the simulation results from CFD with no slip wall conditions. The solid line represents the calculated results with wall slip conditions. All the shape of flow profiles shows a solid-like core enclosed by a fluid-like shell. Due to the wall slip effects, the significant improvement to the topology of the gels structure can be observed. And larger  $\dot{\gamma}_a$  can lead to more significant wall slip, and is more pronounced for gels with higher PEI concentration.

#### Structure dynamics of colloidal inks

Figure 9 shows the equilibrium structural parameter  $\lambda_e$  profiles of three gels as a function of normalized radius position at the nozzle exit under apparent shear rate. These structural parameter curves quantitatively describe gels structures breakage extent. For the same apparent shear rate, the gel with higher PEI concentration owns larger core region, and larger structural parameters at any position. For each gel, larger apparent shear rate leads to stronger structural breakage. At the lower apparent shear rate, there exists a core region and a shear-thinning region outside. At the higher apparent shear rate, the shear-thinning region shrinks very fast, and there is a Newtonian fluid-like region at the outside, where the structural parameter decrease very slow.

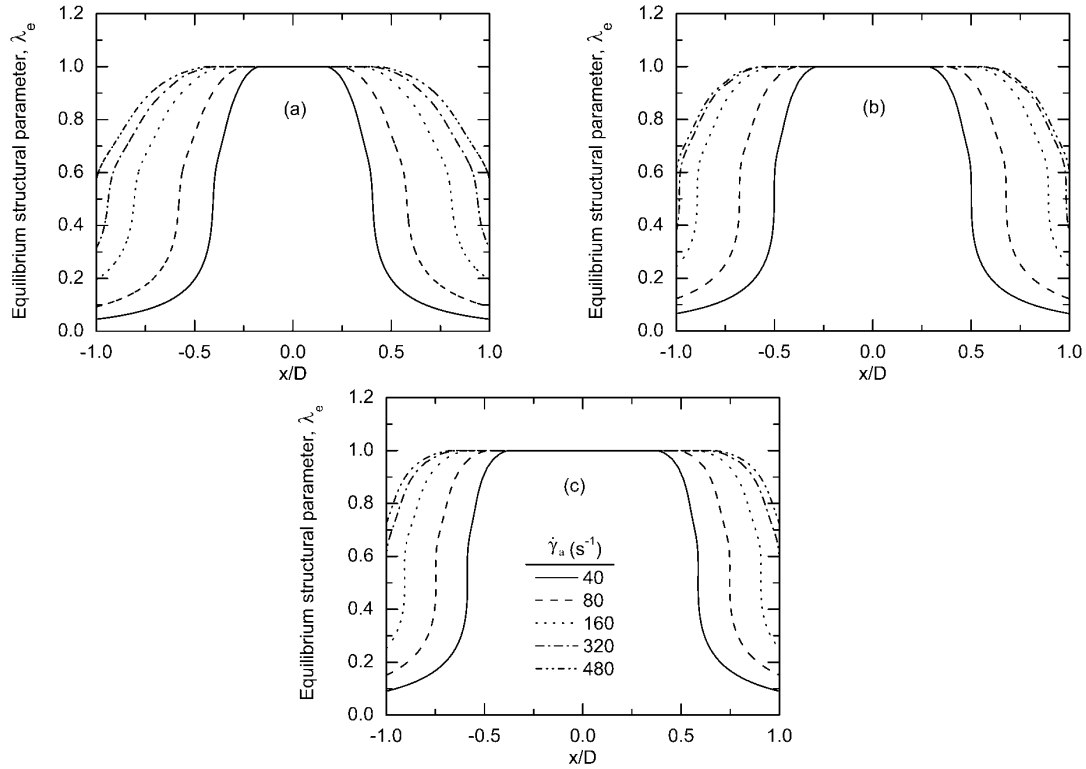


Figure 9 Structural parameter change profile under different apparent shear rate for three gels with varying PEIwt% = (a) 0.010, (b) 0.014, (c) 0.018.

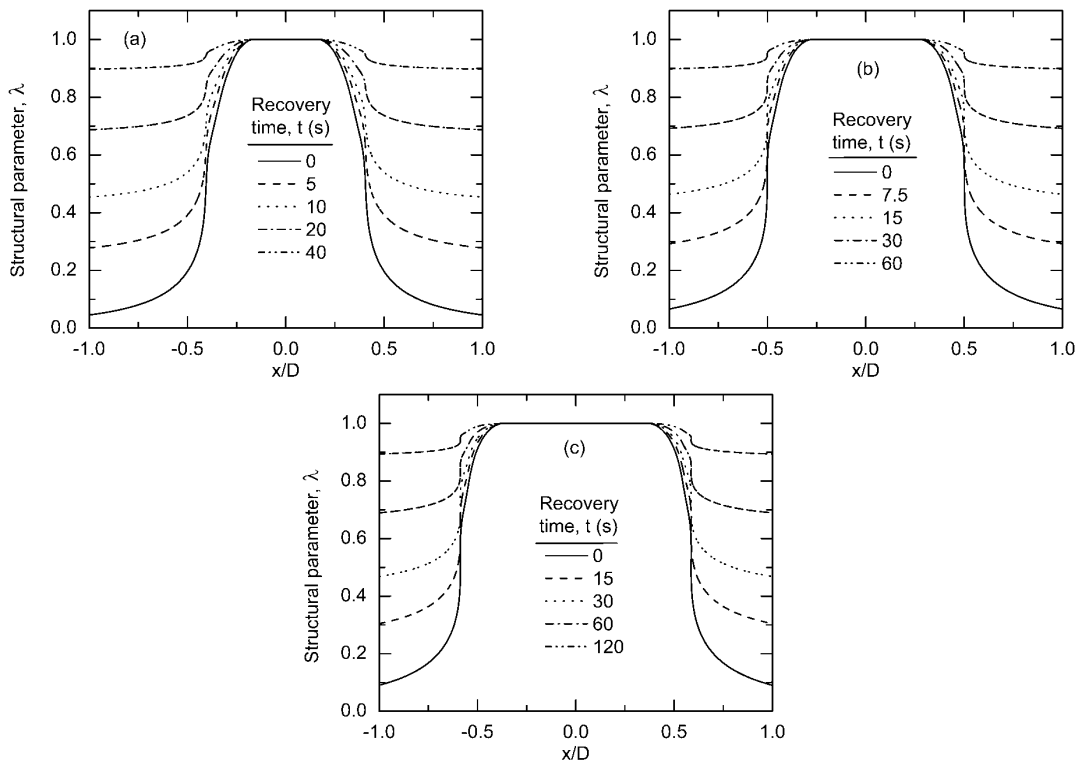


Figure 10 Structure profiles recovery after deposition as a function of time for three gels with varying PEIwt% = (a) 0.010, (b) 0.014, (c) 0.018.

After deposition, the structure of the gel will recover from the initial equilibrium state (i.e.,  $\lambda_i = \lambda_e$ ) to fully structured state ( $\lambda = 1$ ). Integrating Eq. (1) and setting  $\dot{\gamma} = 0$ , the structural parameters evolution equation after cessation of shear flow is given by:

$$\lambda = 1 + (\lambda_i - 1)\exp(-k_0 t) \quad (18)$$

Figure 10 shows the structural parameters recovery as a function of time after deposition at different radial position. The three gels are all deposited at  $\dot{\gamma}_a = 480\text{s}^{-1}$ , and start to reconstruct their network from time  $t = 0$ . In the shear thinning region, the recovery rate slows as the radial position decreases.

### Conclusions

This paper is the first part of a comprehensive project carried out to evaluate the shape evolution of 3D structures fabricated by direct-write assembly. The systematic understanding of complex rheological behavior of colloidal gels can provide necessary information for dynamic flow during deposition and structural recovery after deposition. The thixotropic rheology of  $\text{Al}_2\text{O}_3$  colloidal gels have been observed and confirmed through shear rate step change, and hysteresis loops experiments. By introducing the structural parameter, a thixotropic rheological model for concentrated colloidal gels with viscoelasticity has been developed and applied to the experimental results. The results are in agreement with the predicted values from the model. Our model is simple with few model parameters, and provides better overall simulation results. Extrusion flow dynamics was conducted, and wall slip effect was taken into account to accurately describe the flow dynamics of colloidal gels. The simulation results can convey the rheological information of the colloidal gels flow. The structural parameter was introduced to quantitatively describe the microstructure of the colloidal gels during direct-write process. These results offer new insight into the relationship between flow behavior and gels structure evolution.

### References

1. Smay, J.E., et al., *Directed Colloidal Assembly of 3D Periodic Structures*. Advanced Materials, 2002. **14**: p. 1279-83.
2. Smay, J.E., J. Cesarano, and J.A. Lewis, *Colloidal Inks for Directed Assembly of 3-D Periodic Structures*. Langmuir, 2002. **18**: p. 5429-37.
3. Lee, Y.J. and P.V. Braun, *Tunable Inverse Opal Hydrogel pH Sensors*. Advanced Materials, 2003. **15**(7-8): p. 563-566.
4. Tressler, J.F., et al., *Functional composites for sensor, actuators and transducers*. Composites Part A (Applied Science and Manufacturing), 1999. **30A**(4): p. 477-82.
5. Joannopoulos, J.D., P.R. Villeneuve, and S.H. Fan, *Photonic crystals: putting a new twist on light*. Nature, 1997. **386**: p. 143-9.
6. Therriault, D., S.R. White, and J.A. Lewis, *Chaotic mixing in three-dimensional microvascular networks fabricated by direct-write assembly*. Nature Materials, 2003. **2**(4): p. 265-71.
7. Lin, S.Y., et al., *A three-dimensional photonic crystal operating at infrared wavelengths*. Nature, 1998. **394**: p. 251-53.
8. Smay, J.E., *Direct Colloidal Assembly and Characterization of PZT-Polymer Composite*, in *Material Science and Engineering*. 2002, UIUC: Urbana.
9. Lewis, J.A., *Direct ink writing of 3D functional materials*. Advanced Functional Materials, 2006. **16**: p. 2193-04.
10. Morissette, S.L., et al., *Solid freeform fabrication of aqueous alumina-poly(vinyl alcohol) gelcasting suspensions*. Journal of the American Ceramic Society, 2000. **83**(10): p. 2409-16.

11. Lewis, J.A., *Colloidal Processing of Ceramics*. Journal of the American Ceramic Society, 2000. **83**: p. 2341-59.
12. Roberts, M.T., et al., *Direct Flow Visualization of Colloidal Gels in Microfluidic Channels*. Langmuir, 2007. **23**: p. 8726-31.
13. Conrad, J.C. and J.A. Lewis, *Structure of Colloidal Gels during Microchannel Flow*. Langmuir, 2008. **24**(15): p. 7628-34.
14. Barnes, H.A., *Thixotropy-a review*. Journal of Non-Newtonian Fluid Mechanics, 1997. **70**: p. 1-33.
15. Doraiswamy, D., et al., *The Cox-Merz rule extended: a rheological model for concentrated suspensions*. Journal of Rheology, 1991. **34**: p. 647-685.
16. Yziquel, F., et al., *Rheological modeling of concentrated colloidal suspensions*. Journal of Non-Newtonian Fluid Mechanics, 1999. **86**: p. 133-155.
17. Mujumdar, A., A.N. Beris, and A.B. Metzner, *Transient phenomena in thixotropic systems*. Journal of Non-Newtonian Fluid Mechanics, 2002. **102**: p. 157-178.
18. Dullaert, K. and J. Mewis, *Stress Jumps on Weakly Flocculated Dispersions: Steady State and Transient Results*. Journal of Colloid and Interface Science, 2005. **287**: p. 542-551.
19. Dullaert, K. and J. Mewis, *Thixotropy: Build-up and Breakdown Curves during Flow*. Journal of Rheology, 2005. **49**(6): p. 1213-1230.
20. Dullaert, K. and J. Mewis, *A Structural Kinetics Model for Thixotropy*. Journal of Non-Newtonian Fluid Mechanics, 2006. **139**: p. 21-30.
21. Labanda, J. and J. Llorens, *A Structural Model for Thixotropy of Colloidal Dispersions*. Rheology Acta, 2006. **45**: p. 305-14.
22. Barn, H.A., *A Review of Slip (Wall Depletion) of Polymer Solutions, Emulsions, and Particle Suspensions in Viscometers: Its Cause, Character, and Cure*. Journal of Non-Newtonian Fluid Mechanics, 1995. **56**: p. 221-251.
23. Buscall, R., I.J. McGowan, and A.J. Morton-Jones, *The Rheology of Concentrated Dispersions of Weakly attracting Colloidal Particles With and Without Wall Slip*. Journal of Rheology, 1993. **37**(4): p. 621-41.
24. Mewis, J., *Thixotropy-general review*. Journal of Non-Newtonian Fluid Mechanics, 1979. **6**(1): p. 1-20.
25. Bagley, E.B., *End Correction in the Capillary Flow of Polyethylene*. Journal of Applied Physics, 1957. **28**: p. 624-7.
26. Jastrzebski, Z.D., *Entrance Effects and Wall Effects in an Extrusion Rheometer during the Flow of Concentrated suspensions*. Industrial and Engineering Chemistry Fundamentals, 1967. **6**(3): p. 445-453.
27. Şakar-Deliormanlı, A., E. Çelik, and M. Polat., *Rheological behavior of PMN gels for solid freeform fabrication*. Colloids and Surfaces A: Physicochemical and Engineering Aspects., 2008. **324**(1-3): p. 159-66.
28. Toorman, E.A., *Modeling the thixotropic behavior of dense cohesive sediment suspensions*. Rheology Acta, 1997. **36**: p. 56-65.
29. Chen, J.Y. and Z. Fan, *Modelling of Rheological Behavior of Semisolid Metal Slurries Part 2-Steady State Behavior*. Material Science and Technology, 2002. **18**: p. 243-249.
30. Gautham, B.P. and P.C. Kapur, *Rheological Model for Short Duration Response of Semi-Solid Metals*. Material Science and Engineering A, 2005. **393**: p. 223-228.
31. Kee, D.D. and G. Turcotte, *Viscosity of biomaterials*. Chemical Engineering Communication, 1980. **6**: p. 273-282.